

■ Synthesis Design

***tert*-Butyl(*tert*-butoxy)zinc Hydroxides: Hybrid Models for Single-Source Precursors of ZnO Nanocrystals**

Kamil Sokołowski,^[a] Iwona Justyniak,^[a] Wojciech Bury,^[b] Justyna Grzonka,^[c]
Zbigniew Kaszukur,^[a] Łukasz Mąkowski,^[b] Michał Dutkiewicz,^[b] Agnieszka Lewalska,^[b]
Elżbieta Krajewska,^[b] Dominik Kubicki,^[b] Katarzyna Wójcik,^[a] Krzysztof J. Kurzydłowski,^[c] and
Janusz Lewiński^{*[a, b]}

Dedicated to Professor Stanisław Pasynkiewicz on the occasion of his 85th birthday

Abstract: Alkylzinc alkoxides, [RZnOR']₄, have received much attention as efficient precursors of ZnO nanocrystals (NCs), and their "Zn₄O₄" heterocubane core has been regarded as a "preorganized ZnO". A comprehensive investigation of the synthesis and characterization of a new family of *tert*-butyl(*tert*-butoxy)zinc hydroxides, [(*t*Bu)₄Zn₄(μ₃-OtBu)_x(μ₃-OH)_{4-x}], as model single-source precursors of ZnO NCs is reported. The direct reaction between well-defined [*t*BuZnOH]₆ (**1**) and [*t*BuZnOtBu]₄ (**2**) in various molar ratios allows the isolation of new mixed cubane aggregates as crystalline solids in a high yield: [(*t*Bu)₄Zn₄(μ₃-OtBu)₃(μ₃-OH)] (**3**), [(*t*Bu)₄Zn₄(μ₃-

OtBu)₂(μ₃-OH)₂] (**4**), [(*t*Bu)₄Zn₄(μ₃-OtBu)(μ₃-OH)₃] (**5**). The resulting products were characterized in solution by ¹H NMR and IR spectroscopy, and in the solid state by single-crystal X-ray diffraction. The thermal transformations of **2**–**5** were monitored by in situ variable-temperature powder X-ray diffraction and thermogravimetric measurements. The investigation showed that the Zn–OH groups appeared to be a desirable feature for the solid-state synthesis of ZnO NCs that significantly decreased the decomposition temperature of crystalline precursors **3**–**5**.

Introduction

In the last decade much attention has been given to the development of zinc oxide preparation methods. The demands of modern semiconductor technologies stimulate the quest for new efficient precursors of nanostructured ZnO. Its most advanced precursors are organozinc complexes known as single-source precursors, which contain building blocks with the appropriate stoichiometry of zinc and oxygen ions. In this respect, alkylzinc alkoxides, [RZn(μ₃-OR')]₄, perform very well to yield ZnO nanocrystals (NCs), and their "Zn₄O₄" heterocubane

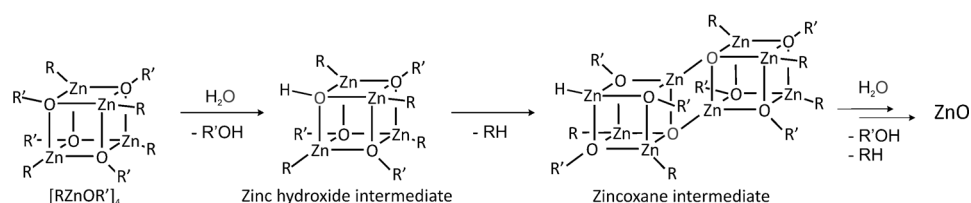
core has been dubbed "preorganized ZnO".^[1,2] These alkoxides form ZnO NCs^[3] either by controlled thermolysis under various conditions^[1,4] or by reaction with H₂O.^[2] The formation of ZnO nanostructures in this type of single-source systems undoubtedly involves a number of consecutive transformations, each of which requires the occurrence of fundamental processes on the molecular level, followed by nanoparticle nucleation and growth. In the case of the hydrolytic transformation of heterocubanes [RZnOR']₄, it is likely that the generation of various intermediary alkyl(alkoxy)zinc hydroxide and oxide clusters occurs. Recent spectroscopic investigations of the reaction between [MeZn(μ₃-OR)]₄ (in which R=Me, Et, Bu, *i*Pr, *t*Bu) and H₂O indicated that the alkoxide group reacted faster than the Zn–Me group.^[2c] On this way to ZnO NCs, the formation of a relatively unstable intermediate, in which the OH groups occupy one edge of the Zn₄O₄ cubane core, followed by its transformation to an edge-sharing oxo(alkoxide) zinc dicubane, was postulated (Scheme 1).^[2c] However, the inability to isolate crystalline samples of these intermediates prevented confirmation of the proposed structures by X-ray diffraction. Interestingly, such mixed compounds, if isolated, could act as excellent single-source precursors of ZnO NCs because their decomposition would be driven by proton transfer from ZnOH species to the zinc-bonded alkyl and/or alkoxide ligands. However, the interaction of organozinc compounds with water remains an area essentially little explored, so far, and the great potential of such reactions for synthesizing useful zinc hydroxides remains

[a] K. Sokołowski, Dr. I. Justyniak, Prof. Z. Kaszukur, Dr. K. Wójcik, Prof. J. Lewiński
Institute of Physical Chemistry, Polish Academy of Sciences
Kasprzaka 44/52, 01-224 Warsaw (Poland)

[b] Dr. W. Bury, Ł. Mąkowski, M. Dutkiewicz, A. Lewalska, E. Krajewska, D. Kubicki, Prof. J. Lewiński
Faculty of Chemistry, Warsaw University of Technology
Noakowskiego 3, 00-664 Warsaw (Poland)
Fax: (+48) 22-3433333
E-mail: lewin@ch.pw.edu.pl
Homepage: <http://lewin.ch.pw.edu.pl>

[c] Dr. J. Grzonka, Prof. K. J. Kurzydłowski
Faculty of Materials Science and Engineering,
Warsaw University of Technology
Wołoska 141, 02-507 Warsaw (Poland)

Supporting information for this article is available on the WWW under <http://dx.doi.org/10.1002/chem.201406245>.



Scheme 1. The proposed hydrolytic transformation pathway of heterocubane-like alkylzinc alkoxides to ZnO NCs.^[2c]

undeveloped.^[5-7, 12] Therefore, it seems reasonable to investigate how a variety of $RZnOR'$ compounds interact with H_2O and how stable the resulting products are.

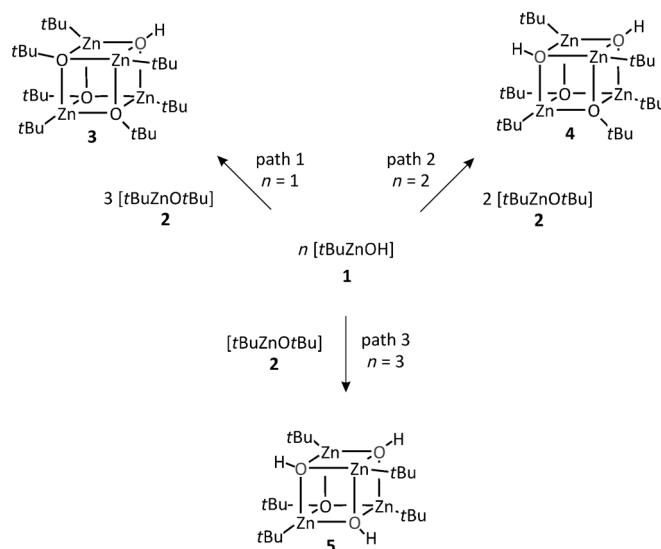
Based on our experience in the synthesis of alkylzinc alkoxides,^[8] hydroxides,^[6a-c,e,8b] and oxides,^[6d,9] herein we describe the efficient synthesis of unique mixed *tert*-butyl(*tert*-butoxy)-zinc hydroxide aggregates, $[(tBu)_4Zn_4(\mu_3-OtBu)_x(\mu_3-OH)_{4-x}]$. These compounds were obtained from a combination of the well-defined molecular alkylzinc hydroxide $[tBuZn(\mu_3-OH)]_6$ (**1**)^[6e] and the corresponding zinc alkoxide $[tBuZn(\mu_3-OtBu)]_4$ (**2**)^[8a]. The resulting alkyl(alkoxy)zinc hydroxides were tested as predesigned precursors in the solid-state synthesis of ZnO NCs by using a combination of thermogravimetric analysis (TGA), variable-temperature powder X-ray diffraction (VT PXRD) and transmission electron microscopy (TEM). The results show that increasing the number of hydroxyl groups within the Zn_4O_4 core significantly decreases the temperature of decomposition of the heterocubane precursors, which reveals the crucial role of Zn–OH species in the hydrolytic pathway to ZnO NCs.

Results and Discussion

Synthesis

To test the hypothesis that mixed heterocubanes containing ZnOH moieties can be formed as intermediate species during the reaction of alkylzinc alkoxides with water,^[2c] we prepared a series of mixed alkoxy(hydroxy)zinc compounds. Initially, we tested the reactivity of previously reported $[tBuZnOtBu]$ (**2**)^[8a] towards H_2O . The reaction of freshly dissolved **2** in toluene (or THF) with an equimolar amount of H_2O was carried out with vigorous stirring. Our attempts to isolate crystalline products of the hydrolysis of **2** failed due to rapid precipitation of an insoluble solid from the post-reaction mixture. These results indicate the high reactivity of **2** towards H_2O , which is in contrast to the much lower reactivity of the isostructural heterocubane $[MeZn(\mu_3-OtBu)]_4$ described by Polarz and co-workers.^[2c] Then, we performed the synthesis by using a different synthetic approach that involved **1** and **2** in various molar ratios (Scheme 2). We found that the mixture of freshly dissolved **1** and **2** in toluene in a molar ratio of 1:3 (based on Zn) afforded reproducibly a novel mixed alkyl(alkoxy)zinc monohydroxide, $[(tBu)_4Zn_4(\mu_3-OtBu)_3(\mu_3-OH)]$ (**3**) (Scheme 2, path 1). From the post-reaction mixture, colorless block-shaped crystals of **3** were grown and isolated in almost quantitative yield. A similar strategy was employed for other homologues of **3** with a higher hydroxyl to alkoxy ratio. We carried out the reac-

tions of **1** and **2** in molar ratios of 1:1 and 3:1 (based on Zn), which led to the formation of $[(tBu)_4Zn_4(\mu_3-OtBu)_2(\mu_3-OH)_2]$ (**4**) and $[(tBu)_4Zn_4(\mu_3-OtBu)(\mu_3-OH)_3]$ (**5**), respectively (Scheme 2, paths 2 and 3). Compounds **3–5** are stable in solution at ambient temperature. Although the



Scheme 2. Synthetic pathways for the crystalline alkyl(alkoxy)zinc hydroxides **3**, **4**, and **5**.

formation of biscubane zincoxanes was postulated previously as a route to the formation of ZnO phase,^[2c] in our reaction systems, neither edge- nor corner-sharing biscubanes^[10] were isolated upon varying the temperature and concentration of the reactants.^[11] However, mono- and biscubane-type zincoxanes were reported for the oxygenation of the $Me_2Zn/1,4$ -diazabutadiene system^[9a] or in the direct hydrolysis of Et_2Zn in the presence of pyridine.^[12]

Structural studies

Compounds **3–5** were characterized in solution by 1H NMR and IR spectroscopy (see the Experimental Section), as well as in the solid state by single-crystal X-ray diffraction analysis. The molecular structures of previously characterized compounds **1**₆^[6e] and **2**₄^[8a] as well as of the new compounds **3–5**, are shown in Figure 1, and selected bonds lengths and angles are given in Table 1. Compound **3** crystallizes in the trigonal $R\bar{3}c$ space group, whereas compounds **4** and **5** crystallize in the triclinic space group $P\bar{1}$. All studied *tert*-butyl(*tert*-butoxy)zinc hydroxide compounds (**3–5**) have a distorted heterocubane structure. In general, their composition can be viewed as that of compound **2** in which *t*BuO moieties were replaced by one, two, or three hydroxide ligands. In all of these structures, each hydroxide ligand bridges to three zinc centers and adopts the

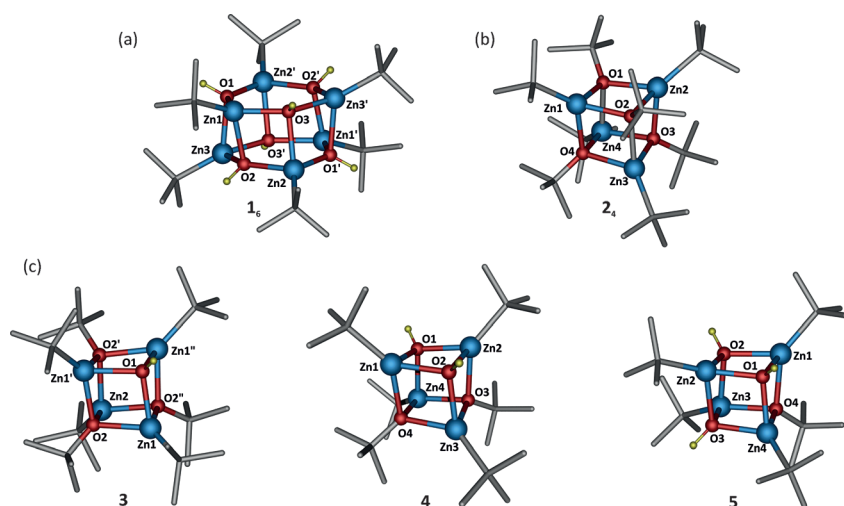


Figure 1. The molecular structures of ZnO NCs precursors a) alkylzinc hydroxide $1_6^{[6e]}$ and b) the alkylzinc alkoxide $2_4^{[8]}$ along with c) the mixed alkyl(alkoxy)zinc hydroxides 3–5; the hydrogen atoms of *tert*-butyl were omitted for clarity.

Table 1. Selected bond lengths [Å] and angles [°] of 1–5.

	$1_6^{[6e]}$	$2_4^{[8]}$	3	4	5
Zn1–O1	2.044(7)	2.109(3)	2.098(8)	2.098(3)	2.086(3)
Zn1–O2	2.184(8)	2.098(3)	2.079(9)	2.046(3)	2.036(3)
Zn2–O1	–	2.116(3)	–	2.047(3)	2.040(3)
Zn2–O2	2.019(8)	2.098(3)	2.137(9)	2.096(3)	2.061(3)
Zn2–O3	2.146(7)	2.121(3)	–	2.083(3)	2.107(3)
Zn3–O2	–	2.109(3)	–	2.070(3)	2.075(3)
Zn3–O3	–	2.105(3)	–	2.100(3)	2.068(3)
Zn4–O1	–	2.116(3)	–	2.070(3)	2.084(3)
Zn1–O1–Zn2	–	96.91(11)	–	95.48(13)	98.10(12)
Zn1–O2–Zn2	94.6(3)	97.41(11)	97.8(3)	95.56(13)	99.06(12)
Zn2–O3–Zn3	–	96.75(11)	–	96.21(13)	94.54(11)
Zn4–O3–Zn3	–	97.36(11)	–	96.74(13)	98.57(12)

μ_3 -OH coordination mode. In the molecular structures of 3–5, two types of Zn–O bonds can be distinguished. The Zn–O bonds that originate from hydroxide groups are in the range of 2.019(8)–2.184(8) Å, whereas bonds involving *tert*-butoxide ligands fall in the range of 2.059(3)–2.100(3) Å. Alternatively, compound 4 can be regarded as an adduct of $[t\text{BuZnOH}]_2$ and $[t\text{BuZnOtBu}]_2$ dimeric units. Similar structural analysis of 3 leads to the conclusion that it can be formed by association of dinuclear $[(t\text{BuZnOH})(t\text{BuZnOtBu})]$ and $[t\text{BuZnOtBu}]_2$ units, whereas 5 is a combination of $[(t\text{BuZnOH})(t\text{BuZnOtBu})]$ and $(t\text{BuZnOH})_2$ moieties. We note that these putative dinuclear units can combine statistically, depending on their relative populations.

Thermogravimetric studies

Alkylzinc alkoxides have been widely employed as single-source precursors of ZnO NCs in thermolytic processes.^[2] In our previous study, we demonstrated that crystalline *tert*-butylzinc hydroxide 1 was a very reactive precursor that decomposed smoothly in one step at 120 °C to form wurtzite-type ZnO NCs (Figure 2).^[6e] Undoubtedly, structurally well character-

ized compounds 1–5 present a good opportunity to verify how the presence of hydroxide ligands can affect the thermal stability and decomposition paths of hydroxyzinc alkoxide complexes. Therefore, we performed TGA studies for alkylzinc alkoxide 2 and the corresponding mixed alkyl(alkoxy)zinc hydroxides 3–5. The TGA profiles for crystalline 1–5 are shown in Figure 2 and Figures S4–S6 in the Supporting Information. The thermolysis of 2–5 under an argon atmosphere (with the heating rate of 2 Kmin⁻¹) showed a significantly more complex decomposition path

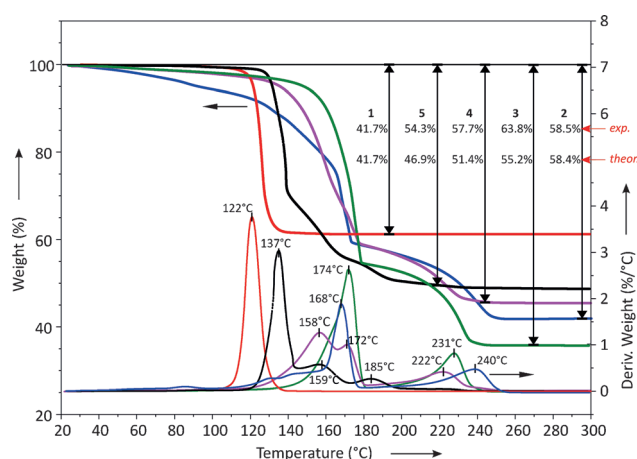


Figure 2. TGA and derivative thermogravimetric analysis (DTG) traces showing the decomposition of compounds 1 (red), 2 (blue), 3 (green), 4 (pink), and 5 (black) in an inert (Ar) atmosphere.

than that observed for 1; however, the TGA curves show two distinct trends. In the TGA profile of 2 (Figure 2) two main decomposition steps are present with a maximum decomposition rate at 168 and 240 °C.^[6e] The decomposition process is finished at about 260 °C with a total weight loss of 58.5%, which is in good agreement with a theoretical value of 58.4% (based on the transformation into ZnO). The TGA profiles of 3 and 4 (Figure 2) exhibit two-step decomposition pathways, very similar to that observed for 2, with their maxima shifted to lower temperatures. In comparison, in the first decomposition step of 4, two overlapping components at 158 and 172 °C can be observed. For 3 and 4, the total weight loss (3 (63.8%), 4 (57.7%)) is higher than the theoretical values (3 (55.2%), 4 (51.4%); based on the transformation into ZnO). This observation can be explained in terms of partial sublimation of the mixed heterocubanes under atmospheric pressure.^[1b] On the other hand, the thermal decomposition profile of 5 is more similar to that of 1, showing one major decomposition step

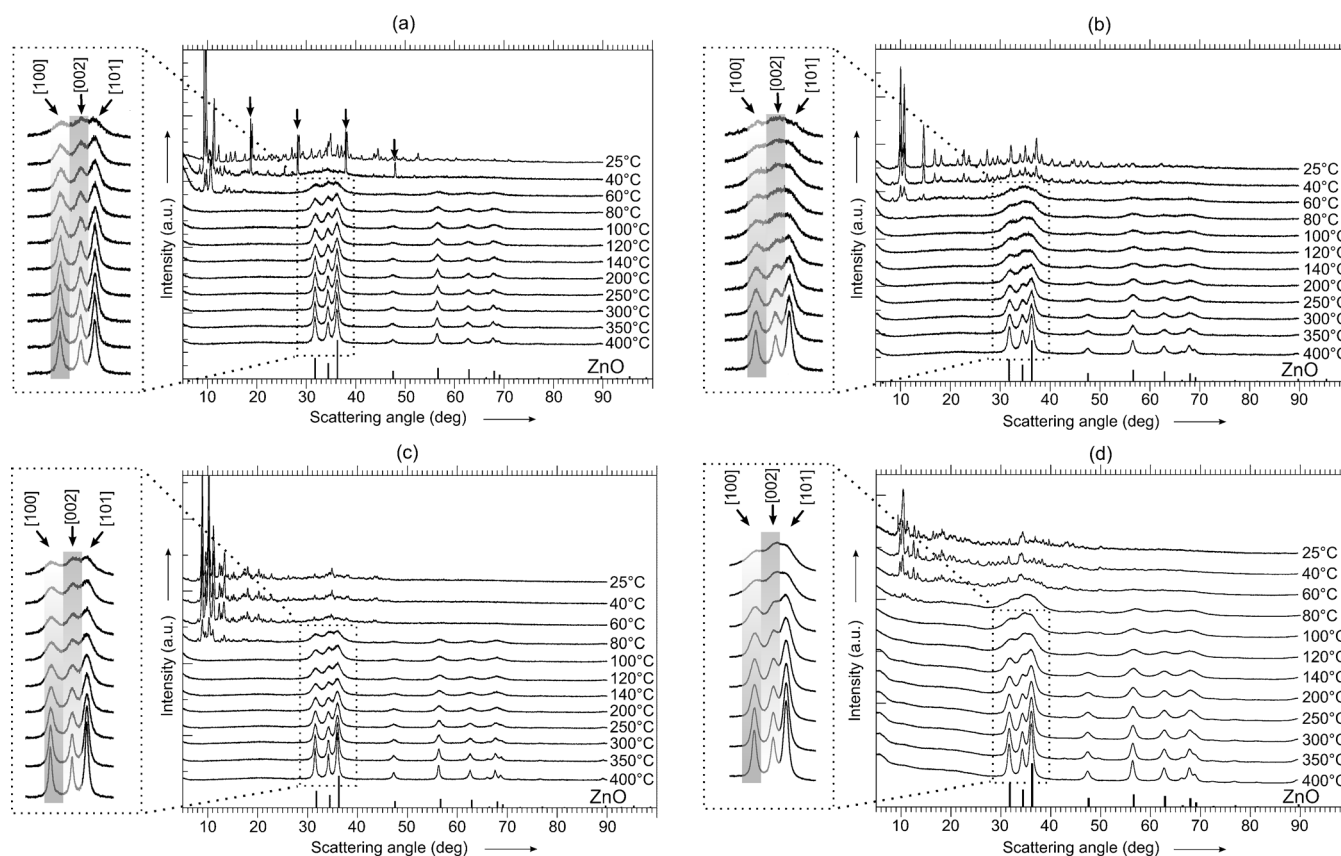


Figure 3. VT PXRD profiles of ground sample of compounds **2** (a), **3** (b), **4** (c), and **5** (d). The insets show changes in the relative intensity of peaks attributed to the [100] and [002] reflections during thermal treatment (the darker gray color of the strips, the higher relative peaks intensity). The arrows indicate some strong reflections as an effect of anisotropic evolution of the original pattern.

with a maximum at 137 °C. These observations suggest that hydroxyl groups present in the structures of compounds **3–5** act as a source of protons required to initiate the decomposition process and significantly decrease the decomposition temperature. Indeed, the decomposition temperatures of **3–5** are considerably lower than the recently reported data for single-source precursors of the [RZnOR]₄-type. The latter precursors exhibited multistep decomposition pathways to ZnO NCs with an upper limit at 350–450 °C.^[2]

VT PXRD studies

There is limited insight into the nature of the early stages of ZnO nucleation and growth in the solid-state transformations of predesigned alkylzinc alkoxide and alkyl(alkoxy)zinc hydroxide precursors with the Zn₄O₄ core.^[1b,c] Having in hand a series of well-defined molecular precursors **2–5**, we decided to follow their stepwise transformation into the ZnO wurtzite phase and the evolution of the forming ZnO NCs during thermolysis by using VT PXRD (Figure 3). All described crystalline precursors were ground just before PXRD measurements were made. Grinding did not cause any changes in the diffraction patterns of the starting materials **2** and **3** relative to those calculated from single-crystal data. These materials are also the most stable ones and decompose at the highest temperatures (see the TGA measurements section). Interestingly, the same proce-

dures applied to **1**, **4**, and **5** resulted in slight changes in their starting PXRD patterns. This can be rationalized in terms of mechanochemically driven transformations of **1**, **4**, and **5** crystal lattices, which can occur during preparation of samples by grinding, and this observation emphasizes the importance of highly reactive O–H groups in solid-state transformations.^[13]

As we reported previously, the VT PXRD analysis of ground sample of **1** showed that the formation of wurtzite-type ZnO nanoclusters starts already at temperatures as low as 60 °C.^[6e] Further heating of the sample led to a slow sintering of as-formed nanoparticles (average diameter of 2.6 and 3.4 nm in the [100] and [002] directions, respectively), resulting in the formation of larger aggregates (average diameter of 4.5 nm at 150 °C and finally 8.0 nm at 450 °C; Table 2 and Figure 4). The growth rate seems to be highest in the [100] direction, initially at the cost of growth in the [002] direction. During thermal decomposition of powdered **2**, the PXRD pattern evolves through molecular rearrangement and causes a decrease and broadening of the Bragg reflections together with slight modifications of the lattice periods, mostly due to thermal expansion (Figure 3a). Interestingly, at 40 °C, some sharp peaks appear, which may belong to the crystallographic system of the original lattice and then at 60 °C ordering typical for wurtzite ZnO starts to be visible along with the remnants of crystalline ordering (Figure 3a). At 80 °C, all periodicities of the original lattice vanish and the only ordering displayed by diffraction is that of

Table 2. Analysis of the crystallite size by means of the Scherrer formula of ZnO NCs derived from 1–5 by temperature treatment.				
	<i>T</i> [°C]	Size [100] [nm]	Size [002] [nm]	Aspect ratio
1	80	2.6	3.4	1.3
	150	4.8	2.4	2.0
	450	8.5	5.5	1.5
2	80	1.8	4.5	2.5
	150	2.9	3.5	1.2
	450	9.7	8.0	1.2
3	80	2.1	3.0	1.4
	150	2.8	3.0	1.1
	450	11.9	9.9	1.2
4	80	3.4	3.0	1.1
	150	4.4	5.6	1.3
	450	18.8	17.4	1.1
5	80	1.6	2.5	1.6
	150	3.7	3.5	1.1
	450	10.8	8.9	1.2

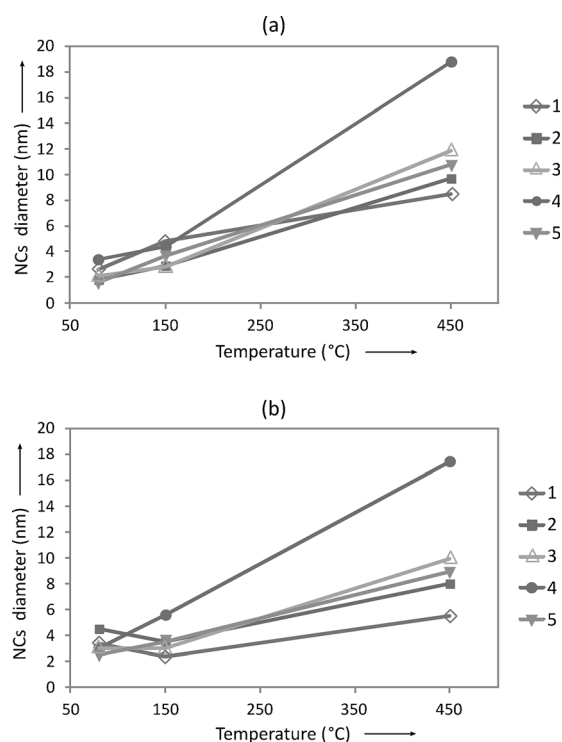


Figure 4. Graphical representation of the changes in the size of ZnO crystallites during the heating procedure in the a) [100] and b) [002] directions.

nanocrystalline wurtzite-type ZnO with average crystallite sizes of less than 2.0 nm in the [100] direction and 4.5 nm in the [002] direction. With increasing temperature, the NCs of ZnO tend to sinter initially mostly in the [100] direction at the expense of the [002] direction to 3.0 nm at 150 °C and 9.0 nm at 450 °C. For powders of **3**, **4**, and **5**, the original periodicity vanishes at around 80 °C with the development of a wurtzite-type ZnO nanostructure with crystallite sizes of 2.5, 3.0, and 2.0 nm, respectively (Figures 3b–d and 4). At 150 °C, the NCs grow to 3.0, 5.0, and 4.0 nm, respectively, and up to 11.0, 18.0, and 10.0 nm at 450 °C, respectively.

The listed crystal size estimates (Table 2 and Figures S12–S15 in the Supporting Information) based on the Scherrer equation were calculated by assuming only a small contribution of the lattice microstrain to peak broadening.^[14] The integral width (ratio of the peak area and its height) was found to be a better measure of the average ordered atomic column length. Analysis of the crystallite sizes shows anisotropy of the forming NCs, typically with the greatest size in the [002] direction. This means that initial growth occurs preferentially on the [002] facets.

During further growth, the size isotropy is usually restored at around 150 °C. However, for **4** this process requires temperatures higher than 200 °C, at which the overall growth rate is highest (up to 18 nm at 450 °C). On the other hand, in the case of **1**, the NCs grow in the [100] direction at the expense of the [002] direction (Figure 4) and this process continues, even at 450 °C. Interestingly, the highest initial anisotropy (at ≈80 °C) of the forming NCs is observed for nanoparticles obtained from **2** (aspect ratio ≈2.5). For precursors that contain –OH groups, aspect ratios of particles formed at about 80 °C are in the range of 0.9–1.6. For **2** at 40–60 °C, we also observe some strong reflections (Figure 3a) that might be the effect of anisotropic evolution of the original pattern. This evolution can be explained in terms of a tendency of molecules to directed rearrangement among the crystal lattices of **2** through planar forms consisting of the nearest molecules. The described intrinsic anisotropy effects can further influence the more anisotropic character of ZnO NCs obtained from **2** compared with these obtained from **3–5** (for these precursors, the network of nearest molecules has a 3D character and decomposition is more isotropic). With a temperature above 300 °C, all samples tend to grow, and lattice microstrain is barely noticeable from Williamson–Hall plots (even large scatter of points around the linear regression line is visible). Because thermal treatment releases the strain, the low-temperature data are probably, to some extent, affected by strain and the crystal size might be underestimated. Also, the observed decomposition temperatures of **2–5** are lower for PXRD than those for TGA. When considering the much longer measurement time for PXRD, this suggests that the decomposition process has long kinetics caused, for example, by entropic barriers.

High-resolution (HR) TEM measurements

To obtain qualitative insights into the structure of the synthesized ZnO nanopowders, we performed HRTEM measurements. The samples were prepared by thermal decomposition of compounds **2–5** under an argon atmosphere (from 30 to 150 °C (2 h) with a heating rate of 2 Kmin^{−1}; a procedure resembling TGA experiments). The HRTEM micrographs in secondary electrons (SE) and transmission modes of the resulting ZnO NCs are presented in Figure 5 and Figures S7–S10 in the Supporting Information.^[15] These micrographs show aggregates of wurtzite-type ZnO NCs, as confirmed by fast Fourier transformations performed on selected particles. The ZnO NC shapes are close to spherical, as confirmed by aspect ratios equal to 1.2, 1.2, 1.1, and 1.1, respectively (see also the PXRD data;

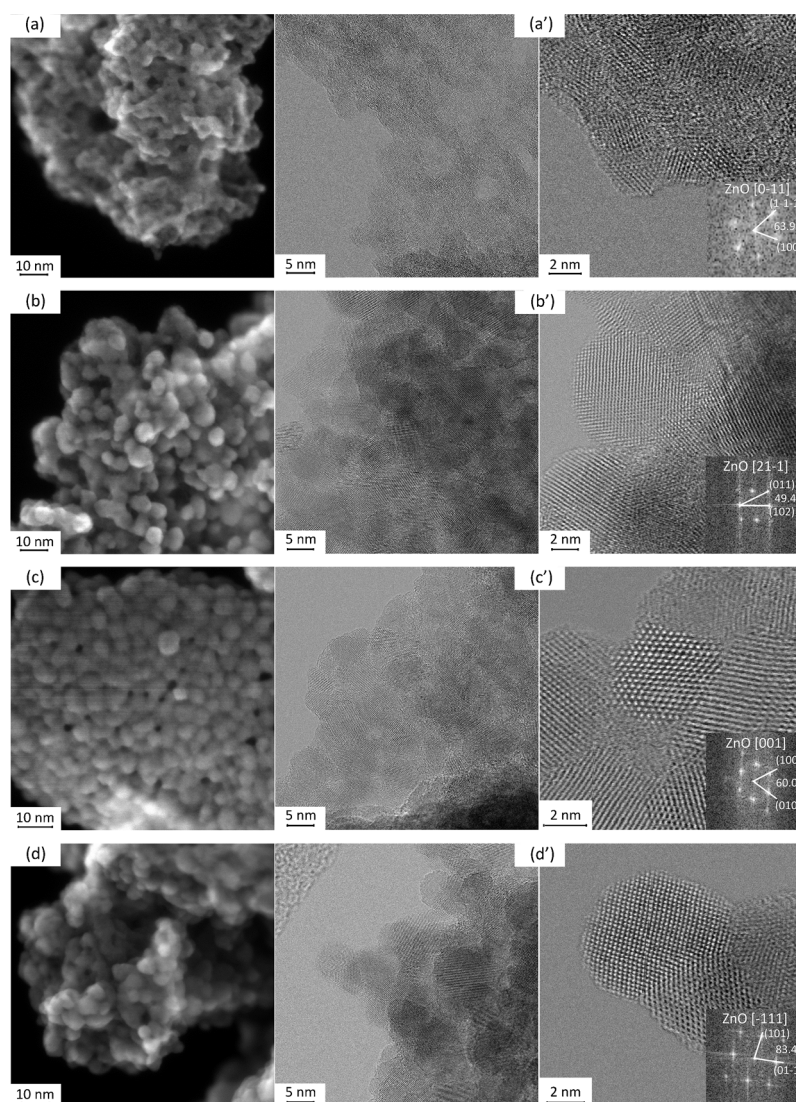


Figure 5. HRTEM micrographs of ZnO NCs in SE (a–d) and transmission (a'–d') modes obtained by thermal decomposition of a) 2, b) 3, c) 4, and d) 5 under an argon atmosphere at 30→150 °C (2 h) with a heating rate of 2 Kmin⁻¹.

Table 2). The mean diameters of nanoparticles derived from heterocubanes **2**, **3**, **4**, and **5** are (3.7 ± 0.8), (7.2 ± 1.7), (5.1 ± 1.1), and (6.3 ± 0.9) nm, respectively (Figure S11 in the Supporting Information). Although they are only qualitative, the presented TEM data confirm the formation of monodispersed NC phases with isotropic morphology of ZnO nanoparticles.

Conclusion

We successfully synthesized, in high yield, a series of the first well-defined mixed cubane alkyl(alkoxy)zinc hydroxides, [(tBu)₄Zn₄(μ₃-OtBu)_x(μ₃-OH)_{4-x}], which were derived from a combination of the well-defined molecular alkylzinc hydroxide **1**₆ and the zinc alkoxide **2**₄. The formation of an edge-sharing oxo(alkoxide) zinc dicubane or other types of bis(cubanes) was not observed upon varying the temperature and concentration of the reactants in the studied systems. The in situ VT PXRD and TGA measurements showed that the hybrid aggregates **3**–

5 (which were considered as intermediates in the hydrolysis of [RZnOR']₄ precursors) decomposed at relatively low temperatures with the formation of wurtzite-type ZnO NCs. This study demonstrated that the Zn–OH functionality in the reported complexes appeared to be a desirable feature that lowered the decomposition temperature of the precursors significantly.

Experimental Section

Materials and methods

All experiments and manipulations were carried out under a dry, oxygen-free nitrogen atmosphere by using standard Schlenk techniques. Di-*tert*-butylzinc was synthesized according to a literature procedure^[16] and purified by careful sublimation in the dark. All other reagents were purchased from commercial vendors. Solvents and *tert*-butyl alcohol were stringently dried and distilled prior to use. Ultrapure water (Millipore, Milli-Q) was degassed by six freeze–pump–thaw cycles and stored under an inert gas. The NMR spectra were acquired on a Varian Mercury 400 MHz spectrometer. IR spectra were obtained by using a PerkinElmer System 2000 FTIR spectrophotometer. Thermal stability experiments were performed in a dry argon atmosphere at a heating rate of

2 Kmin⁻¹ by using open alumina crucibles on a TA Instruments Q600 simultaneous TG-DSC analyzer. PXRD patterns were obtained by using a Siemens D5005 diffractometer (Bruker AXS). Nickel-filtered Cu_{Kα} radiation of a copper sealed tube charged with 40 kV voltage and 40 mA current and a Bragg–Brentano geometry with beam divergence of 1° in the scattering plane was used. In situ measurements were performed by using a stainless-steel camera of our own design with a steel sample holder containing an electric heater and a steel cap with an X-ray window sealed by Kapton tape. The sample was spread over the surface of a porous glass plate fixed to the sample holder. The heating mode of 2 Kmin⁻¹ between measured isothermal steps (1.5 h) was applied. Diffraction patterns were measured in the range of 5–90° of a scattering angle by step scanning with steps of 0.02°. Microscopic structure characterization of the powders was carried out by using a high-resolution scanning transmission electron microscope (Hitachi HD-2700, 200 kV, C_s corrected). The scanning transmission electron microscopy (STEM) observations were carried out in three modes: SE (images used to study morphology), bright-field (BF) STEM (images coupled with diffraction contrast), and HR STEM (images showing

the atomic structure). A wide variety of magnifications (from $\times 1500$ to $\times 8000000$) were used to study the microstructure of ZnO samples. From these images, first indications of the particle structure were obtained. Particle size distributions were calculated by counting the diameters of 100 particles in the lower magnification images, defining size intervals of 0.25 nm between $d_{\min} \leq d \leq d_{\max}$, and counting the number of particles falling into these intervals.

Synthesis of 1 and 2

Compounds **1**^[6e] and **2**^[8] were synthesized according to previously described procedures.

[(tBu)₄Zn₄(μ₃-OtBu)₃(μ₃-OH)] (3)

Compound **1** (0.140 g, 0.17 mmol) in toluene (8.0 mL) was added to a solution of compound **2** (0.587 g, 0.75 mmol) in toluene (8.0 mL). Compound **3** was obtained as colorless crystals after recrystallization from concentrated mixture at 4 °C (0.613 g, 84%). ¹H NMR ([D₈]THF, 400.10 MHz, 298 K): δ = 4.37 (s, 1H; ZnOH), 1.42 (s, 9H; OC(CH₃)₃), 1.23 (s, 18H; OC(CH₃)₃), 1.14 (s, 9H; ZnC(CH₃)₃), 1.09 (s, 9H; ZnC(CH₃)₃), 1.08 ppm (s, 18H; ZnC(CH₃)₃); IR (Nujol, KBr): $\tilde{\nu}$ = 3623 (w), 2944 (s), 2913 (s), 2855 (s), 1473 (m), 1363 (m), 1361 (m), 1221 (w), 1178 (w), 1006 (w), 908 (m), 817 (w), 768 (w), 724 (w), 644 (b), 531 cm⁻¹ (m); elemental analysis calcd (%) for C₂₈H₆₄O₄Zn₄: C 46.29, H 8.88; found: C 46.74, H 8.91.

[(tBu)₄Zn₄(μ₃-OtBu)₂(μ₃-OH)₂] (4)

Compound **1** (0.280 g, 0.34 mmol) in toluene (8.0 mL) was added to a solution of compound **2** (0.390 g, 0.50 mmol) in toluene (8.0 mL). Compound **4** was obtained as colorless crystals after recrystallization from a concentrated mixture at -25 °C (0.590 g, 88%). ¹H NMR ([D₈]THF, 400.10 MHz, 298 K): δ = 4.28 (brs, 1H; ZnOH), 1.34 (s, 9H; OC(CH₃)₃), 1.06 (s, 9H; ZnC(CH₃)₃), 1.01 ppm (s, 9H; ZnC(CH₃)₃); IR (Nujol, KBr): $\tilde{\nu}$ = 3657 (w), 2943 (s), 2920 (s), 2850 (s), 1473 (m), 1374 (m), 1362 (m), 1251 (w), 1181 (w), 1019 (w), 902 (m), 817 (w), 766 (w), 724 (w), 648 (b), 533 cm⁻¹ (m); elemental analysis calcd (%) for C₂₄H₅₆O₄Zn₄: C 43.00, H 8.42; found: C 43.42, H 8.45.

[(tBu)₄Zn₄(μ₃-OtBu)(μ₃-OH)₃] (5)

Compound **1** (0.420 g, 0.50 mmol) in toluene (8.0 mL) was added to a solution of compound **2** (0.195 g, 0.25 mmol) in toluene (8.0 mL). Compound **5** was obtained as colorless crystals after recrystallization from a concentrated mixture at -25 °C (0.455 g, 74%). ¹H NMR ([D₈]THF, 400.10 MHz, 298 K): δ = 4.43 (s, 3H; ZnOH), 1.38 (s, 9H; OC(CH₃)₃), 1.08 (s, 27H; ZnC(CH₃)₃), 1.06 ppm (s, 9H; ZnC(CH₃)₃); IR (Nujol, KBr): $\tilde{\nu}$ = 3645 (w), 2954 (s), 2923 (s), 2855 (s), 1463 (m), 1377 (m), 1367 (m), 1241 (w), 1184 (w), 1008 (w), 916 (m), 814 (w), 763 (w), 721 (w), 642 (b), 536 cm⁻¹ (m); elemental analysis calcd (%) for C₂₀H₄₈O₄Zn₄: C 39.11, H 7.88; found: C 39.56 H 7.92;

Crystallographic data

The data were collected at 100(2) K on a Nonius Kappa CCD diffractometer^[17] by using graphite monochromated MoK_α radiation ($\lambda = 0.71073$ Å). The crystal was mounted in a nylon loop in a drop of silicon oil to prevent the possibility of decay of the crystal during data collection. The unit cell parameters were determined from ten frames, then refined on all data. The data were processed with DENZO and SCALEPACK (HKL2000 package).^[18] The structure was

solved by direct methods by using the SHELXS97^[19] program and was refined by full-matrix least squares on F^2 by using the program SHELXL97.^[20] All non-hydrogen atoms were refined with anisotropic displacement parameters. The hydrogen atoms were introduced at geometrically idealized coordinates with a fixed isotropic displacement parameter equal to 1.5 (methyl groups) times the value of the equivalent isotropic displacement parameter of the parent carbon. CCDC-988961 (**3**), 988962 (**4**), and 988963 (**5**) contain the supplementary crystallographic data for this paper. These data can be obtained free of charge from The Cambridge Crystallographic Data Centre via www.ccdc.cam.ac.uk/data_request/cif.

Crystal data for 3: C₂₈H₆₄O₄Zn₄; $M = 726.35$; crystal dimensions 0.18 × 0.16 × 0.12 mm³; trigonal; space group $R3c$ (no. 161); $a = 16.417(11)$, $b = 16.417(11)$; $c = 23.07(5)$ Å; $U = 5385(16)$ Å³; $Z = 6$; $F(000) = 2304$; $\rho_{\text{calcd}} = 1.344$ g cm⁻³; $T = 100(2)$ K; $\mu(\text{MoK}\alpha) = 2.522$ mm⁻¹; $\theta_{\text{max}} = 25.02^\circ$; 1994 unique reflections; 117 parameters; $R1 = 0.0776$; $wR2 = 0.1461$ ($R1 = 0.1125$, $wR2 = 0.1573$ for all data); $\text{Goof} = 1.084$.

Crystal data for 4: C₂₄H₅₆O₄Zn₄; $M = 670.25$; crystal dimensions 0.24 × 0.16 × 0.10 mm³; triclinic; space group $P\bar{1}$ (no. 2); $a = 10.4449(4)$, $b = 11.0031(6)$; $c = 15.6302(7)$ Å; $\alpha = 76.894(2)^\circ$; $\beta = 74.711(3)^\circ$; $\gamma = 68.254(3)^\circ$; $U = 1592.63(13)$ Å³; $Z = 2$; $F(000) = 704$; $\rho_{\text{calcd}} = 1.552$ g cm⁻³; $T = 100(2)$ K; $\mu(\text{MoK}\alpha) = 2.999$ mm⁻¹; $\theta_{\text{max}} = 24.71^\circ$; 5212 unique reflections; 289 parameters; $R1 = 0.0464$; $wR2 = 0.1110$ ($R1 = 0.0588$, $wR2 = 0.1169$ for all data); $\text{Goof} = 1.057$.

Crystal data for 5: C₂₀H₄₈O₄Zn₄; $M = 614.14$; crystal dimensions 0.28 × 0.18 × 0.14 mm³; triclinic; space group $P\bar{1}$ (no. 2); $a = 10.5071(5)$, $b = 10.6149(5)$; $c = 14.9211(7)$ Å; $\alpha = 76.125(2)^\circ$; $\beta = 69.630(2)^\circ$; $\gamma = 68.009(2)^\circ$; $U = 1435.07(12)$ Å³; $Z = 2$; $F(000) = 640$; $\rho_{\text{calcd}} = 1.421$ g cm⁻³; $T = 100(2)$ K; $\mu(\text{MoK}\alpha) = 3.321$ mm⁻¹; $\theta_{\text{max}} = 27.47^\circ$; 5851 unique reflections; 268 parameters; $R1 = 0.0462$; $wR2 = 0.1101$ ($R1 = 0.0539$, $wR2 = 0.1135$ for all data); $\text{Goof} = 1.073$.

ZnO nanoparticle preparation for TEM experiments

Nanocrystalline materials were prepared by thermolysis of crystalline precursors **1–5** in a quartz tube oven. Degradation was carried out under an argon atmosphere at 30 °C → 150 °C (2 h) with a heating rate of 2 K min⁻¹.

TEM sample preparation

Nanocrystalline ZnO materials were suspended in THF by using an ultrasonic bath (5 min). Then, the microscopic samples were prepared by droplet coating of suspensions of ZnO NCs in THF on copper grids covered with carbon film.

Acknowledgements

We acknowledge the Foundation for Polish Science Team Programme co-financed by the EU "European Regional Development Fund" TEAM/2011-7/8 and the National Science Centre (Grant DEC-2011/01/B/ST5/06338) for financial support. K.W. thanks the Nanotechnology, Biomaterials and alternative Energy Source for ERA integration (REGPOT-CT-2011-285949-NOBLESSE) Project from the EU.

Keywords: alkoxides • hydroxides • zinc • zinc oxide

- [1] a) J. Auld, D. J. Houlton, A. C. Jones, S. A. Rushworth, M. A. Malik, P. O'Brien, G. W. Critchlow, *J. Mater. Chem.* **1994**, *4*, 1249–1253; b) S. Polarz, A. Roy, M. Merz, S. Halm, D. Schroeder, L. Schneider, G. Bacher, F. E. Krus, M. Driess, *Small* **2005**, *1*, 540–552; c) V. Ischenko, S. Polarz, D. Grote, V. Stavarache, K. Fink, M. Driess, *Adv. Funct. Mater.* **2005**, *15*, 1945–1954; d) S. Polarz, J. Strunk, V. Ischenko, M. W. E. van den Berg, O. Hinrichsen, M. Muhler, M. Driess, *Angew. Chem. Int. Ed.* **2006**, *45*, 2965–2969; *Angew. Chem.* **2006**, *118*, 3031–3035; e) S. Polarz, R. Regenspurger, J. Hartmann, *Angew. Chem. Int. Ed.* **2007**, *46*, 2426–2430; *Angew. Chem.* **2007**, *119*, 2478–2482.
- [2] a) T. J. Boyle, S. D. Bunge, N. L. Andrews, L. E. Matzen, K. Sieg, M. A. Rodriguez, T. J. Headley, *Chem. Mater.* **2004**, *16*, 3279–3288; b) S. Polarz, F. Neues, M. W. E. van den Berg, W. Grunert, L. Khodeir, *J. Am. Chem. Soc.* **2005**, *127*, 12028–12034; c) C. Lizandara-Pueyo, M. W. E. van den Berg, A. De Toni, T. Goes, S. Polarz, *J. Am. Chem. Soc.* **2008**, *130*, 16601–16610; d) C. Lizandara-Pueyo, S. Siroky, S. Landsmann, M. W. E. van den Berg, M. R. Wagner, J. S. Reparaz, A. Hoffmann, S. Polarz, *Chem. Mater.* **2010**, *22*, 4263–4270; e) M. Krumm, C. Lizandara-Pueyo, S. Polarz, *Chem. Mater.* **2010**, *22*, 5129–5136; f) C. Lizandara-Pueyo, S. Siroky, M. R. Wagner, A. Hoffmann, J. S. Reparaz, M. Lehmann, S. Polarz, *Adv. Funct. Mater.* **2011**, *21*, 295–304; g) S. Polarz, A. V. Orlov, F. Schüth, A.-H. Lu, *Chem. Eur. J.* **2007**, *13*, 592–597.
- [3] Notably, the controlled transformations of these Zn₃O₂ alkylzinc alkoxides yield nano-ZnO of high purity and controlled oxygen vacancies, which determine the catalytic, electrical, optoelectronic, and photochemical properties of semiconducting nanostructures (cf. ref. [1c,d]).
- [4] C. G. Kim, K. Sung, T. M. Chung, D. Y. Jung, Y. Kim, *Chem. Commun.* **2003**, 2068–2069.
- [5] D. Prochowicz, K. Sokołowski, J. Lewiński, *Coord. Chem. Rev.* **2014**, *270*, 112–126.
- [6] For recent examples of implications of R₂Zn/H₂O systems in materials chemistry, see: a) K. Sokołowski, W. Bury, I. Justyniak, D. Fairen-Jimenez, K. Sołtys, D. Prochowicz, S. Yang, M. Schröder, J. Lewiński, *Angew. Chem. Int. Ed.* **2013**, *52*, 13414–13418; *Angew. Chem.* **2013**, *125*, 13656–13660; b) K. Sokołowski, W. Bury, I. Justyniak, A. M. Cieślak, M. Wolska, K. Sołtys, I. Dzięcielewska, J. Lewiński, *Chem. Commun.* **2013**, *49*, 5271–5273; c) K. Sokołowski, I. Justyniak, W. Śliwiński, K. Sołtys, A. Tulewicz, A. Kornowicz, R. Moszyński, J. Lipkowski, J. Lewiński, *Chem. Eur. J.* **2012**, *18*, 5637–5645; d) W. Bury, I. Justyniak, D. Prochowicz, A. Rola-Noworyta, J. Lewiński, *Inorg. Chem.* **2012**, *51*, 7410–7414; e) W. Bury, E. Krajewska, M. Dutkiewicz, K. Sokołowski, I. Justyniak, Z. Kaszkur, K. J. Kurzydowski, T. Płociński, J. Lewiński, *Chem. Commun.* **2011**, *47*, 5467–5469; f) K. Sokołowski, W. Bury, A. Tulewicz, A. M. Cieślak, I. Justyniak, D. Kubicki, E. Krajewska, A. Milet, R. Moszyński, J. Lewiński *Chem. Eur. J.* **2015**, DOI: 10.1002/chem.201406271.
- [7] a) M. Shim, P. Guyot-Sionnest, *J. Am. Chem. Soc.* **2001**, *123*, 11651–11654; b) M. Monge, M. L. Kahn, A. Maisonnat, B. Chaudret, *Angew. Chem. Int. Ed.* **2003**, *42*, 5321–5324; *Angew. Chem.* **2003**, *115*, 5479–5482; c) M. L. Kahn, M. Monge, V. Colliere, F. Senocq, A. Maisonnat, B. Chaudret, *Adv. Funct. Mater.* **2005**, *15*, 458–468; d) M. L. Kahn, M. Monge, E. Snoeck, A. Maisonnat, B. Chaudret, *Small* **2005**, *1*, 221–224; e) C. Pagès, Y. Coppel, M. L. Kahn, A. Maisonnat, B. Chaudret, *ChemPhys-Chem* **2009**, *10*, 2334–2344; f) M. L. Kahn, A. Glaria, C. Pages, M. Monge, L. S. Macary, A. Maisonnat, B. Chaudret, *J. Mater. Chem.* **2009**, *19*, 4044–4060.
- [8] a) J. Lewiński, M. Dutkiewicz, M. Lesiuk, W. Śliwiński, K. Zelga, I. Justyniak, J. Lipkowski, *Angew. Chem. Int. Ed.* **2010**, *49*, 8266–8269; *Angew. Chem.* **2010**, *122*, 8442–8445; b) Ł. Mąkowski, K. Zelga, R. Petrus, D. Kubicki, P. Zarzycki, P. Sobota, J. Lewiński, *Chem. Eur. J.* **2014**, *20*, 14790–14799.
- [9] a) J. Lewiński, K. Suwała, M. Kubisiak, Z. Ochal, I. Justyniak, J. Lipkowski, *Angew. Chem. Int. Ed.* **2008**, *47*, 7888–7891; *Angew. Chem.* **2008**, *120*, 8006–8009; b) J. Lewiński, M. Kościelski, K. Suwała, I. Justyniak, *Angew. Chem. Int. Ed.* **2009**, *48*, 7017–7020; *Angew. Chem.* **2009**, *121*, 7151–7154; c) J. Lewiński, K. Suwała, T. Kaczorowski, M. Gałęzowski, D. T. Gryko, I. Justyniak, J. Lipkowski, *Chem. Commun.* **2009**, 215–217; d) J. Lewiński, W. Bury, M. Dutkiewicz, M. Maurin, I. Justyniak, J. Lipkowski, *Angew. Chem. Int. Ed.* **2008**, *47*, 573–576; *Angew. Chem.* **2008**, *120*, 583–586; e) K. Zelga, M. Leszczyński, I. Justyniak, A. Kornowicz, M. Cabaj, A. E. H. Wheatley, J. Lewiński, *Dalton Trans.* **2012**, *41*, 5934–5938; f) J. Lewiński, M. Dranka, W. Bury, W. Śliwiński, I. Justyniak, J. Lipkowski, *Angew. Chem. Int. Ed.* **2008**, *47*, 573–576; *Angew. Chem.* **2008**, *120*, 583–586; g) D. Prochowicz, K. Sokołowski, I. Justyniak, A. Kornowicz, D. Fairen-Jimenez, T. Friščić, J. Lewiński, *Chem. Commun.* **2015**, 10.1039/c4cc09917f.
- [10] J. Lewiński, W. Marciniak, I. Justyniak, J. Lipkowski, *J. Am. Chem. Soc.* **2003**, *125*, 12698–12699, and references therein.
- [11] For a cooperative effect of dioxygen and water influence on the molecular structure of alkylzinc alkoxides derived from the oxygenation of ZnR₂ compounds, see: S. Jana, R. J. F. Berger, R. Fröhlich, T. Pape, N. W. Mitzel, *Inorg. Chem.* **2007**, *46*, 4293–4297.
- [12] A. Pettersen, A. Lennartson, M. Hakansson, *Organometallics* **2009**, *28*, 3567–3569.
- [13] Notably, the related mechanical treatment of crystals of a metastable trimeric [tBuZnOtBu]₃ cluster led effectively to the stable cubane [tBuZnOtBu]₄ (see ref. [8]). However, issues concerning mechanochemical transformations of organozinc compounds are beyond the scope of this work and will be the subject of further investigations.
- [14] The exact contribution is difficult to determine due to the anisotropy of broadening; for linearization of Williamson–Hall plot, see: a) V. D. Mote, Y. Purushotham, B. N. Dole, *J. Theor. Appl. Phys.* **2012**, *6*, 6; b) G. K. Williamson, W. H. Hall, *Acta Metall.* **1953**, *1*, 22–31. The limited number of resolved peaks is prone to a large error. The microstrain is likely to be significant for ZnO obtained by low-temperature thermolysis of the organometallic precursor (see ref. [1c]). However, a very slow rate of the process employed in VT PXRD experiments (one scan lasting 1.5 h and the whole temperature range is covered in more than 1 day) may substantially diminish the effect of chemical defects.
- [15] For HRTEM data for sample 1, see ref. [6e].
- [16] J. Lewiński, M. Dranka, W. Bury, W. Śliwiński, I. Justyniak, J. Lipkowski, *J. Am. Chem. Soc.* **2007**, *129*, 3096–3098.
- [17] *KappaCCD Software*; Nonius, B. V.: Delft, The Netherlands, **1998**.
- [18] Z. Otwinowski, W. Minor, *Methods Enzymol.* **1997**, *276*, 307–326.
- [19] G. M. Sheldrick, *Acta Crystallogr. Sect. A* **1990**, *A46*, 467–473.
- [20] G. M. Sheldrick, University Göttingen, Germany, **1997**.

Received: November 26, 2014
Published online on February 16, 2015